Discovery of X-ray and Extreme Ultraviolet Emission from Comet C/Hyakutake 1996 B2

C. M. Lisse, K. Dennerl, J. Englhauser, M. Harden, F. E. Marshall, M. J. Mumma, R. Petre, J. P. Pye, M. J. Ricketts, J. Schmitt, J. Trümper, R. G. West

During its close approach to Earth, comet C/Hyakutake 1996 B2 was observed at extreme ultraviolet and x-ray wavelengths with the Röntgen X-ray Satellite and Rossi X-ray Timing Explorer. The emission morphology was symmetric with respect to a vector from the comet's nucleus toward the sun, but not symmetric around the direction of motion of the comet with respect to interplanetary dust. A slowly varying emission and a large impulsive event that varied on time scales of 1 to 2 hours were observed. An interaction between the comet and the solar wind/solar magnetic field seems to be the most likely mechanism for the observed emission.

The close perigee [minimum geocentric distance $\Delta = 0.102$ AU (astronomical unit)] of the long-period comet C/Hyakutake 1996 B2 at universal time (UT) 25.3 March 1996 presented a unique opportunity to search for unusual and low luminosity phenomena in the comet. We searched for emission from the comet at wavelengths where cometary emission was unknown, in the x-ray, using the Röntgen X-ray Satellite (ROSAT) (1) high-resolution imager (HRI) and wide-field camera (WFC) (2), and using the Rossi X-ray Timing Explorer (XTE) proportional counter array (PCA) (3). Appreciable x-ray emission from an object is usually associated with the presence of a hot plasma, highly energetic particles, or with material optically thick enough to scatter x-rays from a nearby external source. We were motivated by the work of Ibadov (4), who predicted that x-rays should be generated by high-speed collisions between dust released by the comet and particles in the interplanetary dust (IPD) cloud, and by the observation of a large number of energetic electrons in the ionosphere of comet P/Halley during the 1986 flybys (5). Prior to our work, only comet Bradfield 1979X had been intentionally observed by an x-ray detector, the Einstein X-ray Observatory imaging proportion-

al counter (IPC) (6); no emission was detected from this comet at a geocentric distance of 0.47 AU, with a 5σ upper limit to the x-ray luminosity of 1.1×10^{14} ergs s^{-1} in the 0.2- to 4.0-keV bandpass (7).

Observations of x-rays in Hyakutake. Pre-perihelion, Hyakutake entered the ROSAT observing window (solar elongation from 75° to 105°) on UT 26 March 1996 and left it on UT 29 March 1996. We obtained 20 ks of time for ROSAT observations of Hyakutake, which took place during nine intervals between UT 26 to 28 March 1996 (Table 1). The HRI and WFC detected the comet in the .09- to 2.0-keV band against the instrumental and cosmic backgrounds. No detection of the comet was made by the PCA on UT 31 March 1996.

WFC and HRI images (Fig. 1) were created by correcting the position of each photon for the motion of the comet across the field of view (FOV), and then smoothing

the result using a 9 × 9 pixel gaussian filter (8). The HRI and WFC images show a similar pattern. The emission is clearly offset sunward in all images but one [this observation was of short duration and thus low signal to noise (S/N) (Table 1)], with a symmetry with respect to the sun-comet line, and an intensity that is variable on a time scale of 1 to 2 hours. This time scale is shorter than the 6.2-hour rotation period of the nucleus (9) and is also shorter than the minimum coma crossing time of ~7 hours (assuming a gas velocity of 0.8 km s^{-1}) for material emitted by the nucleus. The viewing geometry was such that the sun-comet-Earth angle was close to 90°, so that foreshortening of the comet's tail was not important. Compared to optical emission from the comet, the x-ray and extreme ultraviolet (EUV) emissions are offset toward the sun. The spatial extent of the flux in the HRI and WFC images is about the same out of about 50% of the peak brightness in each image, though the low-level emission in the WFC images is much more extended and can be traced out to >200,000 km from the nucleus in the brighter images (Fig. 2). The brightness centroid versus time for the x-ray emission is stable at ~18,000 km sunward of the nucleus and a few thousand km below the sun-comet line, while the intensity of the x-ray flux is variable (Figs. 3 and 4).

Light curves were produced from the HRI and WFC observations by counting all photons within an aperture of a 120,000-km radius [the aperture defined by the spatial extent of our HRI observation on UT 28.42 March (Fig. 4)]. The light curves show an impulsive cometary x-ray emission with up to 13 counts s^{-1} and a variability on 1- to 2-hour time scales superimposed on a slowly varying level of emission at ~4 counts s^{-1}. The WFC light curve is similar to the HRI, although the WFC emission appears softer during the UT 27 March outburst, suggest-

C. M. Lisse is in the Astronomy Department, University of Maryland, College Park, MD 20742, and NASA Goddard Spaceflight Center, Greenbelt, MD 20771, USA. K. Dennerl, J. Englhauser, J. Schmitt, and J. Trümper are at the Max-Planck-Institut für Extraterrestriche Physik, Postfach 1603, 85740 Garching, Germany. M. Harden and M. J. Ricketts are in the Space and Astrophysics Division, Rutherford Appleton Laboratory, Chilton, Didcot, Oxon, OX11 0QX, UK. F. E. Marshall, M. J. Mumma, and R. Petre are at the NASA Goddard Spaceflight Center, Greenbelt, MD 20771, USA. J. P. Pye and R. G. West are in the Department of Physics and Astronomy, University of Leicester, University Road, Leicester, LE1 7RH, UK.

Table 1. Observational geometry, exposure time, and observed counts.

Observation time*	r (AU)	Δ (AU)	Exposure time (s)	(Count/s)‡	
				HRI	WFC
26.52	1.017	0.109	2921	6.27	0.113
26.65	1.014	0.111	3009	8.93	0.174
26.71	1.013	0.112	2872	5.86	0.00907
26.89	1.008	0.115	897	3.14	0.0803
27.57†	0.994	0.125	2303	14.9	0.444
27.71†	0.990	0.130	3009	10.2	0.249
27.78†	0.989	0.131	2642	19.2	0.554
27.84†	0.987	0.133	1556	16.1	0.501
28.43†	0.975	0.146	1295	7.20	0.138
31.28†	0.913	0.222	16	N/A	N/A

*Observation time for UT March 1996 in hours.   †Outburst.   ‡Count rates scaled for distance variations by Δ^{-2}.   March 31.28: PCA observation, count rate was <10.5 counts/s (2 to 10 keV, 3σ upper limit).   March 26.71: High HRI noise.   March 26.89, 28.43: Short exposure times, low S/N.

ing that two different emission mechanisms may produce the slowly varying and impulsive emission. Assuming an average photon energy of 0.25 keV in the HRI bandpass, the total luminosity L_x of the slowly varying emission is 4×10^{15} ergs s^{-1}, about 6000 times the luminosity of the moon as measured by ROSAT (10).

The PCA scanned across Hyakutake on UT 31.28 March 1996. Three of the five on-board detectors recorded the energy and time of each detected x-ray photon. No evidence for x-ray emission from the comet was seen, but upper limits were found for the high-energy tail of the x-ray emission (11, 12). A crude "spectrum" created by combining the HRI, WFC, and PCA photon count rates for the slowly varying emission from Hyakutake (Fig. 5) is consistent with thermal bremsstrahlung models with kT = 0.2 to 0.7 keV or with power-law models with $dN/dE \sim E^{-\Gamma}$, where Γ = 2.2 to 2.5. An HRI flux due solely to fluorescent line emission does not fit the data (13).

Possible mechanisms for the cometary x-rays. One possible mechanism for the observed radiation is fluorescent scattering of solar x-rays by material in the comet's coma. This mechanism has been shown to be active on the moon (10) and would produce soft x-rays, consistent with the PCA upper limits. Assuming that the comet has a composition similar to the sun for atomic number $Z > 2$, then the bulk of the scattering

should be produced by carbon atoms at an energy of 0.28 keV or oxygen atoms at an energy of 0.53 keV. The maximum emission seen in the HRI and WFC images is not at the nucleus, where the column density of carbon and oxygen is highest, but is displaced sunward. One possible explanation for the observed morphology is that we are observing an optically thick shell of material around the nucleus illuminated from the direction of the sun. The shell must be moving at a velocity of less than 0.02 km s^{-1} with respect to the nucleus in order to explain the lack of movement of the brightness centroid seen in the images, implying that the material was emitted more than 10 days before

the observation period. The rapid variability seen on UT 27 March 1996 would be due not to changes in the density of material flowing sunward from the nucleus, but to rapid changes in the solar x-ray flux.

There are serious problems with this model. The mass of material required to reach an optical depth $\tau = 1$ in a shell of material with radius of 18,000 km is $\sim 1 \times 10^{15}$ g [assuming a photo-ionization cross section of 1×10^{-18} cm^2 per atom (14)]. Assuming a conservative density of 0.5 g cm^{-3} for the comet's nucleus, the total mass of the comet is $2 \times 10^{15}\ r_n^3$ where r_n is the radius of the comet's nucleus in kilometers. The mass of material typically shed by comets throughout an apparition is
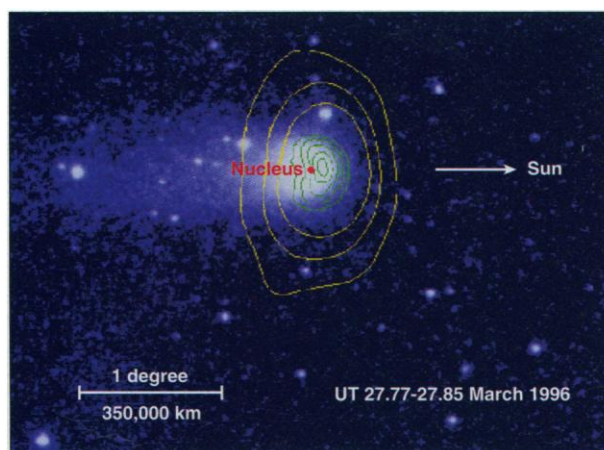

Fig. 2. Overlay of the UT 27.8 March 1996 HRI contours (green) and WFC contours (yellow) on a visible light image of the comet taken on UT 27.8 March 1996. The coordinate system is the same as in Fig. 1. The contour levels are 35, 50, 65, 80, and 95% of the peak HRI emission, and 10, 20, and 30% of the peak WFC flux.
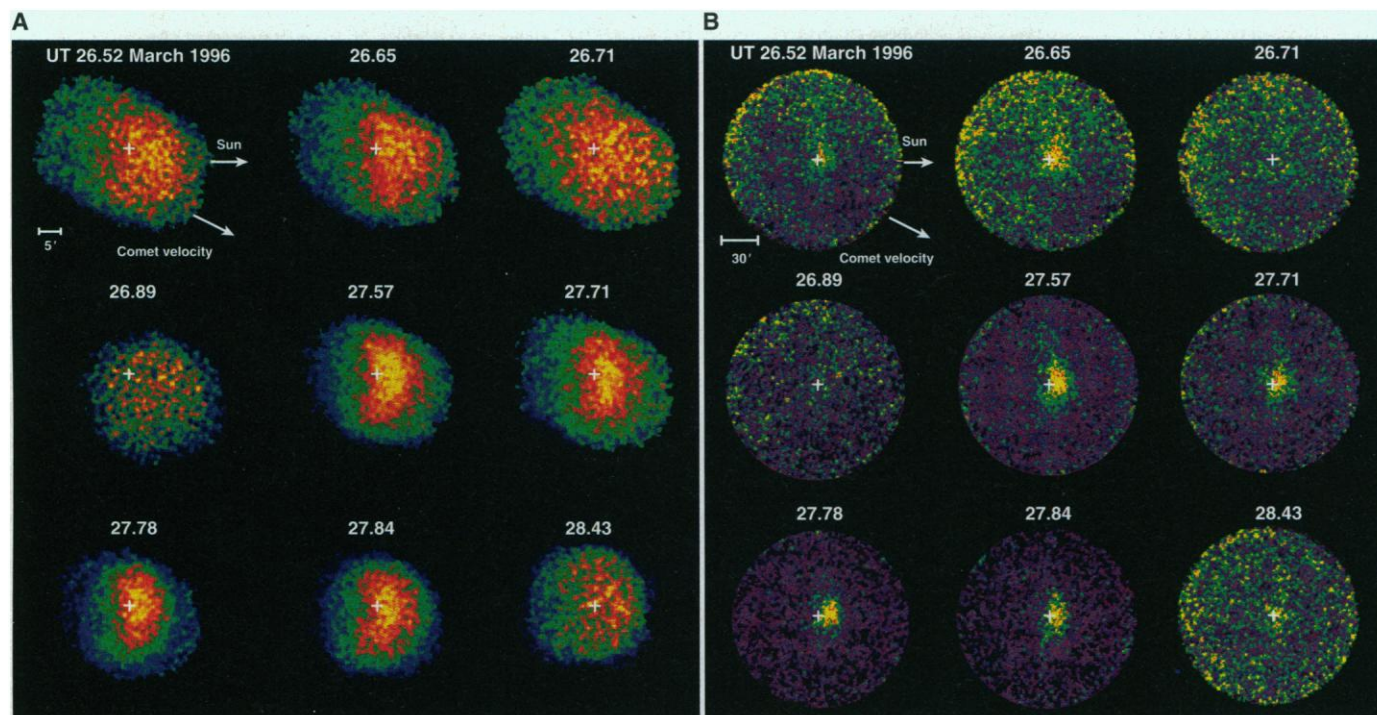

Fig. 1. Time series of (**A**) HRI 0.1 to 2.0 keV x-ray and (**B**) WFC .09 to 0.2 keV EUV images of Hyakutake on UT 26 to 28 March 1996 (Table 1). The images are in a reference frame moving with the comet's apparent sky position. The projected direction toward the sun and the orbital velocity of the comet are shown by arrows. The emission intensity has been autoscaled to the maximum level in each image to produce the highest contrast.

$\ll 1\%$ of the total cometary mass, implying that r_n must be >7 km to have at most 1% of its emitted mass in an optically thick shell. However, the observations of Hyakutake in the infrared and the radio wavelengths (15,16) suggest that the nucleus has a radius of 1 to 3 km. Further, although it is remotely possible that some sort of explosive event sent a large fraction of the comet's mass sunward, it is improbable that such an event would be so symmetrically placed around the sun-comet line. No optically thick shell is seen in Hubble Space Telescope (HST) images of the comet (17), nor do the production rates of water, CS, NH, or dust show any evidence of such an event (9, 18). Comparison of our HRI and WFC light curves with the solar x-ray flux measured by the Geostationary Observational Environmental Satellite–8 (GOES-8) satellite (19) shows no correlation—the solar x-ray flux is relatively low during the cometary x-ray outburst on UT 27 March 1996. Finally, the bulk of the observed x-rays should be in the carbon and oxygen lines, while the observed spectrum is consistent with continuum-dominated emission (Fig. 5).

A related mechanism, scattering of solar x-rays by attogram-size dust, has similar problems. Whereas the amount of mass required for this mechanism depends inversely on the Rayleigh scattering efficiency, which can be quite high, the expected morphology for the emission should be similar to that of dust particles in the coma and tail of the comet. The spectrum of the observed emission is similar to the solar continuum and should track the temporal behavior of the solar x-ray flux, unlike our observations.

A second possible mechanism is that high relative velocity impacts between cometary and the IPD create a soft x-ray–emitting plasma (4). Dust-dust collisions should produce an emission morphology symmetric
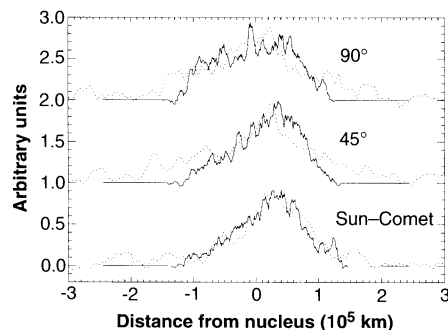
about the velocity of the IPD particles with respect to the comet. Assuming that the bulk of the dust particles are moving at velocities similar to Earth's (that is, with small inclination to the ecliptic versus Hyakutake's large inclination of 124.9°), the velocity direction subtends an angle of $\sim25°$ with respect to the sun-comet direction. Since the maximum emission seen in the HRI images is not at the nucleus, but is displaced sunward from the maximum dust density in the comet, the cometary dust must be optically thick with respect to scattering from the IPD at 18,000 km. However, Ibadov (4) estimates that the region of the comet that is opaque to scattering by the IPD has a radius <100 km. Because the observed emission is stationary with respect to the nucleus, the rapid variability seen on UT 27 March 1996 must be due to changes in the density of the IPD on length scales of ~50 km s^{-1} * 1 hour = 180,000 km; the spatial structure of the IPD is poorly understood. Although the dust-dust mechanism produces a soft x-ray continuum similar to our observations, the predicted luminosity of 7×10^{14} ergs s^{-1} is smaller than the 4×10^{15} ergs s^{-1} observed in the slowly varying emission. Another simple test of this mechanism was performed when we reacquired the comet post-perihelion, on UT 22 to 23 June 1996. After perihelion, the orbital velocity of the comet shifts $\sim180°$ with respect to the sun-comet direction, and the offset of emission from the nucleus should also shift by $\sim180°$ if dust-dust collisions are the production mechanism. No shift was observed in the observed x-ray emission in June 1996.

A third possible mechanism is that the x-ray emission is derived from energy depo-
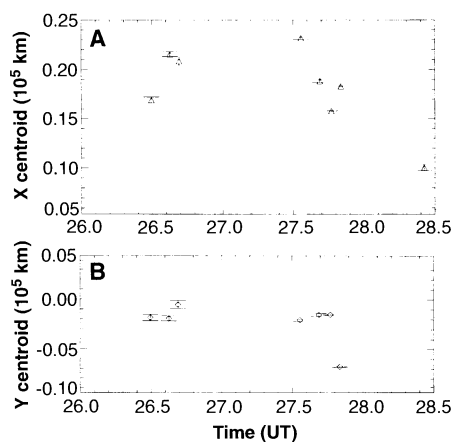
sition by solar wind particles. In this model, the sunward position of the x-ray emission is due to the concentration of hot electrons between the comet's bowshock and contact surface (the boundary between the neutral coma and ionosphere). The position of the bowshock and contact surface in Hyakutake can be inferred from the P/Halley encounters, scaling the distances by the ratio of the production rates of gas in Hyakutake versus P/Halley (20). This ratio is ~5 and is accurate to within a factor of 2 (18). Using this method, Hyakutake's contact surface should be at ~1000 km from the nucleus, the bowshock at $\sim100,000$ km (5, 21), and the x-ray emission should be located between the two (Fig. 2). The slight offset of the emission centroid below the sun-comet line by 5° may be due to the aberration of the solar wind by the comet's orbital velocity, about a 3° effect in the same direction. The rapid variability observed on UT 27 March 1996 may be explained as variations in the solar wind density; similar variations were seen in UV emission from the ionosphere of P/Halley (22). A large enhancement in the solar x-ray flux was observed by GOES 8 on UT 22 to 23 March 1996 (23); the arrival time for any particles associated with the outburst and moving at the 300 to 500 km s^{-1} velocity of the solar wind is 3.5 to 5.8 days later. Soft continuum x-rays would dominate the bremsstrahlung emission generated from the $\sim10^6$ K solar wind ions, consistent with the PCA upper limits and continuum dominated emission seen in the HRI and WFC observations.

A related emission mechanism is disruption of the current flow in the cometary magnetosphere by sector boundary crossings or solar flares. The emission should be concentrated between the bowshock and ionosphere boundary, and have a maximum near the "magnetic pileup region", $\sim30,000$ to 40,000 km sunward for Hyakutake (Fig. 2). Hudson et al. (6) have argued that the total magnetic energy stored in a comet is $\sim4 \times$
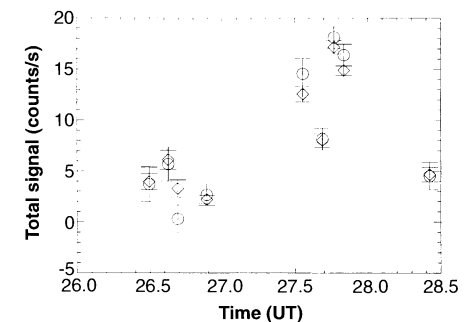

Fig. 3. Profiles of the UT 27.8 March 1996 HRI and WFC images of the comet. The profiles have been offset vertically for presentation purposes. Solid curves: HRI x-ray profiles. Dotted curves: WFC EUV profiles. The profiles at $-45°$ (not shown) are similar to the $+45°$ profile, demonstrating the symmetry of the emission about the nucleus.

Fig. 4. Brightness centroids of the x-ray emission with respect to the nucleus versus time for the nine ROSAT observations. (**A**) The $+x$ direction is toward the sun, and the (**B**) $+y$ direction is above the sun-comet line. The centroids of the two short exposures (not shown) are skewed due to systematic effects.

Fig. 5. X-ray and EUV cometary light curves for Hyakutake taken on UT 26 to 28 March 1996. All error bars are ±2-σ. s: HRI, 0.1 to 2.0 keV light curve (open diamonds). WFC .09 to .20 keV light curve (open circles) scaled by a factor of 32.

$10^{22} L^3$ ergs, which can be disrupted on time scales of ~1000 s, for a total power output of ~4×10^{19} (L ergs s^{-1}, where L is the plasma tail length in 10^6 km). The microphysics of energy transfer and current disruption are, however, unclear. Assuming $L = 18 \times 10$ km (50° apparent length on the sky) and a conversion efficiency into bremsstrahlung x-rays of ~2×10^{-8}, we can account for the observed slowly varying emission. A higher conversion efficiency or power is necessary to explain the rapidly varying emission of UT 27 March 1996. However, no large solar magnetic field changes or disconnection events in the tail of Hyakutake were observed UT 26 to 28 March 1996. Also, while we can expect large amounts of radio emission from large-scale disruptions of the comet's magnetosphere (24), Fernandez et al. (25) and Minter and Langston (26) have reported no detection of the comet to the few hundred millijansky (1 Jy = 10^{-26} W m^{-2} Hz^{-1}) level at 8.35 and 14.35 GHz on UT 26 to 27 March 1996.

The major difficulty with the solar wind/ magnetic field emission models is the lack of a plausible detailed emission mechanism. If one assumes thermal bremsstrahlung as the mechanism, then for $T \sim 10^5 - 10^6$ K, $L_x \sim 1 \times 10^{-23} N_e N_t V$, where N_e is the hot electron density, N_t the target ion density, and V is the volume of the emit-

ting region. For the observed luminosity of ~ 4×10^{15} erg s^{-1}, and a spherical emission region with radius of 60,000 km, $N_e N_t \sim 4 \times 10^8$ cm^{-6} (5, 22). Current models of ion density derived from the P/Halley encounters suggest ion and electron temperatures in this range, but have electron densities $N_e \sim 10 - 100$ cm^{-3} and target densities $N_t \sim 10^3 - 10^4$ cm^{-3} at distances scaled to the maximum of emission seen at Hyakutake. There is, however, enough uncertainty in our current understanding of the complex interaction between cometary ionospheres and the solar wind/ magnetic field that regions of locally enhanced electron energy and density due to shock heating, Fermi acceleration, and magnetic field reconnection may exist (27, 28).

Other comets. Prompted by our discovery of x-ray emission from Hyakutake, Dennerl et al. (29) have searched the archive of the ROSAT x-ray all-sky survey, conducted in 1990–91 with the Position Sensitive Proportional Counter (PSPC) instrument (1). This search has resulted in the discovery of x-ray emission from comets C/Tsuchiya-Kiuchi 1990XVII, C/Levy 1990XX, C/Arai 1990XXVI and 45P/ Honda-Mrkos-Padjusakova 1990, including all three of the brightest comets observed in the ROSAT all-sky survey. The PSPC spectrum of these comets is consistent with thermal bremsstrahlung emission with kT ~0.4 keV, and pure line emission due to oxygen or carbon fluorescence is ruled out, consistent with our results for Hyakutake. The observation of x-ray emission from three more comets along with the persistent detection of emission from Hyakutake postperihelion supports our argument that comets are a class of x-ray luminous objects.
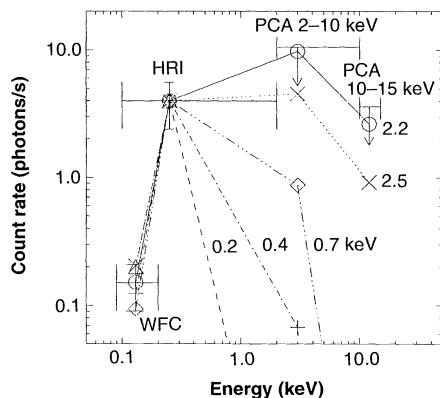
REFERENCES AND NOTES

1. J. Trümper, *Adv. Space. Res.* **2**, 241 (1983).
2. J. H. M. M. Schmitt, *ibid.* **11**, 125 (1991). The ROSAT HRI is a microchannel plate detector coupled to a grazing incidence telescope with an effective area of ~20 cm^2 at 0.1 to 2.0 keV, a circular FOV 38' in diameter, and an angular resolution of 6 inches HEW (half-energy width) (1, 2). Coarse pulse height discrimination is used to distinguish UV sources from x-ray emitting objects. The ROSAT WFC has three concentric gold-plated mirrors coupled to a curved microchannel plate at the focal plane, providing a circular FOV of 5° in diameter with an angular resolution of 2' HEW [M. R. Sims *et al.*, *Opt. Eng.* **29**, 649 (1990) and J. P. Pye *et al.*, *Mon. Not. R. Astron. Soc.* **274**, 1165. (1995)]. All of our WFC observations were obtained with the S1A filter, with a nominal bandpass (at 10% of peak effective area) of 90 to 206 eV and an on-axis effective area of ~1 cm^2. Lack of contamination from UV red leaks (wavelength >1000 Å) has been established by the non-detection of the bright A0 star Vega at a 90% confidence upper limit of 5×10^{-4} counts s^{-1}. The optical axes of the HRI and WFC are co-aligned to within 10 to 15', providing simultaneous observations in the EUV and x-ray. The backgrounds in both instruments are dominated by particles, and must be removed by modeling [S. L. Snowden, personal communication and R. G. West, Thesis, University of Leicester (1993)].
3. The XTE PCA consists of five non-imaging multiwire proportional counters and has an effective area of about 6500 cm^2 [W. Zhang *et al.*, in *Proc. SPIE* **2006**, 324 (1993)]. The PCA detects x-rays in the 2- to 60-keV band with an FOV diameter of about 2°. Background confusion noise dominates the observations in the PCA.
4. S. Ibadov, *Icarus* **86**, 283 (1990).
5. H. Reme, *et al.*, *Astron. Astrophys.* **187**, 33 (1987).
6. H. S. Hudson, W-H. Ip, D. A. Mendis, *Planet. Space Sci.* **29**, 1373 (1981).
7. Whatever mechanism is responsible for the emission of x-rays from comets, it must be highly variable among comets or over time, since the Einstein IPC 5-σ upper limit on the 0.2 to 4.0 keV emission from C/Bradfield (5) is a factor of 70 below our lowest measured flux for Hyakutake in March 1996. after correcting for distance effects. The non-detection of C/Bradfield cannot be explained by large secular changes in solar x-ray flux, since the sun was near the maximum of the solar cycle and its x-ray emission in 1980. and near the minimum in 1996.
8. Corrections for variations in exposure over the comet images were made by modeling the comet's motion across the detector FOV. Background maps were created using the well-characterized spacecraft models of Snowden and West (3). Comparison of the model background to the average total background measured over many orbits gave good agreement. The uncertainties in the light curve are dominated by an ~5% uncertainty in the absolute value of the instrumental backgrounds.
9. D. Schleicher *et al.*, *IAU Circular 6372* (1996).
10. J. H. M. M. Schmitt *et al.*, *Nature* **349**, 583 (1991).
11. The flux in the 2 to 10 keV band was estimated by averaging the count rate [16.75 counts per second (cps)] during the 16-s when the PCA optical axis was closest to the comet's position, subtracting the average rate during the rest of the maneuver (16.01 cps), and dividing by the mean collimator efficiency (0.663) during the observation. We have assumed that the emission from the comet had the same physical size as during the ROSAT observation.
12. A 90% confidence upper limit of 4.5 cps was calculated by adding 1.645 times the standard deviation of the average count rate for other 16-s intervals (1.38 cps), and thus includes variations due to fluctuations of the x-ray sky. Similarly, the 90% confidence limit for the 10 to 15 keV band is 1.54 cps. 3-σ upper limits were then calculated from the 90% confidence limit values by assuming gaussian behavior and multiplying by a factor of (3.0/1.28).
13. In this case the HRI/WFC count rate ratio would be >3000, while the observed ratio is <50.
14. W. J. Veigele, *Atomic Data* **5**, 51 (1973).
15. C. M. Lisse *et al.*, in preparation.
16. S. Ostro, personal communication.
17. H. A. Weaver, personal communication.
18. M. Haken and M. F. A'Hearn, personal communication.
19. GOES-8 data obtained from the World Wide Web at http://web.ngdc.noaa.gov/stp/GOES/goes.html.
20. H. U. Schmidt. personal communication.
21. H. Balsiger *et al.*, *Nature* **321**, 330 (1986).
22. M. Neugebauer *et al.*, *Astron. Astrophys.* **187**, 21 (1987).
23. The GOES-8 spacecraft is located in geosychronous orbit inside the Earth's magnetosheath, and monitors the solar x-ray flux, solar wind, and solar magnetic field. However, Hyakutake was outside the Earth's magnetosheath, where the solar wind and magnetic field are very different. Thus, GOES-8 data can only give us pertinent information about the solar x-ray flux at the comet. The WIND spacecraft, another monitor of the solar wind, was also inside the magnetosheath at the end of March 1996. The IMP-8 spacecraft farther away from the Earth and comet was outside the magnetosheath, and has shown that there were no large changes in the solar magnetic field during UT 26 to 28 March 1996.
24. Another efficient production mechanism for radio frequency emission associated with x-ray luminous objects, synchrotron emission, is unimportant since $L_{x\ synchrotron} \sim B^2$ and cometary magnetic fields are

Fig. 6. Photon count rates of the slowly varying emission of Hyakutake from the HRI, WFC, and PCA observations. The 90% energy widths of the instrumental passbands are given by the horizontal error bars. The average photon energy in each passband has been calculated using a photon index $\Gamma = 2.5$ power law. The HRI and WFC observations have 10% (2σ) error bars due to background subtraction uncertainties. The arrows at 2 to 10 keV are 3-σ upper limits from the PCA measurement of UT 31.3 March 1996, scaled to a geocentric distance of 0.127 AU. Thermal bremsstrahlung fits to the data with plasma temperature kT = 0.2 (open triangles), 0.4 (crosses), and 0.7 keV (open diamonds). Power-law fits to the data with photon index $\Gamma = 2.2$ (open circles) and 2.5 (X's). All models have been scaled to a rate of 4 HRI counts/s.

small, $B_{comet} < 10^{-4}$ gauss.

25. Y. R. Fernandez et al., in preparation.
26. A. H. Minter and G. Langston,. Astrophys. J. Lett. 467, L37 (1996).
27. M. Neugebauer. Rev. Geophys. 28, 231 (1990).
28. T. I. Giombosi, K. Lorencz, J. R. Jokipii, J. Geophys. Res. 94, 15011 (1989).
29. K. Dennerl et al., IAU Circular 6404, 6413 (1996); K. Dennerl et al., in preparation.
30. The authors are indebted to M. D. Desch, Y. R. Fernandez, J. Harrington, T. A. Livengood, D. A. Mendis, T. Northrup, H. U. Schmidt, S. L. Snowden, and D. K. Yeomans for their help and many useful

An αβ T Cell Receptor Structure at 2.5 Å and Its Orientation in the TCR-MHC Complex

K. Christopher Garcia, Massimo Degano, Robyn L. Stanfield, Anders Brunmark, Michael R. Jackson, Per A. Peterson, Luc Teyton, Ian A. Wilson*

The central event in the cellular immune response to invading microorganisms is the specific recognition of foreign peptides bound to major histocompatibility complex (MHC) molecules by the αβ T cell receptor (TCR). The x-ray structure of the complete extracellular fragment of a glycosylated αβ TCR was determined at 2.5 angstroms, and its orientation bound to a class I MHC–peptide (pMHC) complex was elucidated from crystals of the TCR-pMHC complex. The TCR resembles an antibody in the variable Vα and Vβ domains but deviates in the constant Cα domain and in the interdomain pairing of Cα with Cβ. Four of seven possible asparagine-linked glycosylation sites have ordered carbohydrate moieties, one of which lies in the Cα-Cβ interface. The TCR combining site is relatively flat except for a deep hydrophobic cavity between the hypervariable CDR3s (complementarity-determining regions) of the α and β chains. The 2C TCR covers the class I MHC H-2K^b binding groove so that the Vα CDRs 1 and 2 are positioned over the amino-terminal region of the bound dEV8 peptide, the Vβ chain CDRs 1 and 2 are over the carboxyl-terminal region of the peptide, and the Vα and Vβ CDR3s straddle the peptide between the helices around the central position of the peptide.

T lymphocytes respond to a wide variety of foreign antigens that are presented as peptides in the context of major histocompatibility molecules (MHC) (1). Specific recognition of peptide-MHC (pMHC) complexes is accomplished by a membrane-bound, multicomponent, cell surface glycoprotein termed the T cell receptor (TCR). The TCR complex consists of highly diverse, clonotypic αβ or γδ heterodimers and the γ, δ, ε, and ζ chains of the invariant accessory protein CD3 (2). The α and β chains participate in the interaction with the pMHC complex, whereas the CD3 chains partici-

K. C. Garcia, M. Degano, R. L. Stanfield, and I. A. Wilson are at the Department of Molecular Biology and the Skaggs Institute of Chemical Biology, Scripps Research Institute, 10550 N. Torrey Pines Road, La Jolla, CA 92037, USA. A. Brunmark, M. R. Jackson, P. A. Peterson, and L. Teyton are at the R. W. Johnson Pharmaceutical Research Institute–La Jolla, 3535 General Atomic Court, San Diego, CA 92121, USA.

*To whom all correspondence should be addressed. E-mail: wilson@scripps.edu

pate in signal transduction. The genes encoding the TCR resemble immunoglobulin (Ig) genes not only in sequence, but in their assembly by somatic rearrangement of linked variable (V), diversity (D), joining (J), and constant (C) gene segments during lymphocyte development (3, 4). The formation of functional α chain polypeptide requires the in-frame rearrangement of a V-region gene segment to a J-region gene segment, whereas functional β chain polypeptide is formed by two successive rearrangements of V-, D-, and J-region gene elements (5). The rearranged V-J and V-D-J regions are then attached to their respective C regions to assemble the mature α and β chain gene products. A vast number of potential protein sequences can result from these recombinations (4), as with Igs. Although not as striking as in Igs, four regions of hypervariable amino acid sequence are found on both the α and β chains, three of which are analogous to the

antibody complementarity-determining regions (CDRs) (6), which serve as the primary contact points between antibody and antigen (7). Both CDRs 1 and 2 are encoded within the V genes; CDR3 occurs at the V-J junction in the α chain and at the V-D-J junction in the β chain (4).

The high degree of sequence identity between various V and C elements of TCRs and Igs (30 to 70 percent) suggested that TCR domains are folded into β-sheet sandwich structures (8, 9), resembling Ig domains (10), that would pair in a manner similar to the heavy (H) and light (L) chains of antibodies. However, the recognition requirements of a TCR are more restricted than that of an antibody. Antibodies can bind ligands of extensive chemical and structural diversity, as reflected in the different shapes of antibody combining sites, from flat surfaces to deep grooves (7). The function of the TCR is to discriminate among different peptide antigens embedded in the largely flat, undulating surfaces of MHC molecules, whose dimensions and shape are relatively constant. Therefore, a more conserved binding site topology among different TCRs could be expected. Limited sequence diversity of the CDRs 1 and 2 suggested that most of the peptide specificity of the TCR would reside in CDR3, which is the most variable because of the junctional diversity of the V(D)J recombination (4). Site-directed mutagenesis studies confirmed that substitutions in CDR3 can either alter antigen specificity or abolish the response (11). Various models have been proposed for TCR recognition of pMHC in which the CDR3s of Vα and Vβ contact the peptide, whereas CDRs 1 and 2 interact primarily with the MHC α helices (4, 12, 13) or the ends of the peptide (14).

The x-ray structures of an individual TCR β chain from a T cell clone termed 14.3.d (15) and an isolated Vα fragment from a T cell clone termed 1934.4 (16) have confirmed that the TCR does indeed contain Ig-like domains. The Vα and Vβ domains resemble a v-type Ig fold (17), whereas Cβ more distantly resembles a c-type Ig fold (17). The monomeric β chain was proposed to be rather rigid because of extensive contacts between Vβ and Cβ, and a large protruding loop from Cβ that might limit "elbow" motion between Vβ and Cβ domains (15). Both CDRs 1 and 2 appear to be conformationally restricted by main-chain interactions with framework residues but, in the absence of the buttressing effect of their respective α and β chains, the CDR3s fold away from the domain surface toward the solvent.

The absence of a TCR αβ heterodimer crystal structure until now has been due to difficulties in producing large quantities of